POLITECNICO DI TORINO
Repository ISTITUZIONALE

A modal based reduction technique for wide loose interfaces and application to a turbine stator

Availability:
This version is available at: 11583/2843520 since: 2020-08-31T13:12:53Z

Publisher:
Elsevier

Published
DOI:10.1016/j.ymssp.2019.106415

Terms of use:

This article is made available under terms and conditions as specified in the corresponding bibliographic description in the repository

(Article begins on next page)

24 April 2024

A modal based reduction technique for wide loose interfaces and application to a turbine stator

G. Battiato[a,*], C. M. Firrone[a]

[a]*Politecnico di Torino, Department of Mechanical and Aerospace Engineering, Corso Duca degli Abruzzi, 24, 10129 Torino*

Abstract

Aim of this research is the prediction of the non-linear forced response of a stator bladed disk for aeronautical applications in the presence of friction contacts at the hook joints (casing - vane segment contact). Due to the large extension of the contact interfaces the use of classic node-to-node contact elements based on the Coulomb friction law becomes cumbersome. Although such approach appears convenient for problems involving small contact regions, it is computationally expensive when large contact interfaces with refined meshes are present between components. In this research, a novel modal interface reduction method is combined with a layer of Jenkins contact elements in order to efficiently predict the effects of friction on the non-linear forced response of the stator bladed disk. The wide rail/hook contact regions are therefore suitable for the application of the presented technique. The goodness of the proposed methodology is quantified both in terms of accuracy and time costs savings on the calculation of non-linear forced responses by exploiting cyclic symmetry hypotheses and the Harmonic Balance Method.

Keywords: Component Mode Synthesis, Interface reduction methods, Dynamic coupling, Cyclic symmetry, Non-linear forced response, Contact mechanics, Harmonic balance method.

---

*Corresponding author
Email address:* `giuseppe.battiato@polito.it` (G. Battiato)

1. INTRODUCTION

Forced vibrations in resonance conditions might shorten life and reliability of aircraft engines being responsible of high cycle fatigue (HCF) phenomena. Among several sources of dynamic excitation the traveling wave engine order (EO) type are the commonest [1, 2, 3]. In regular operation conditions turbine blade arrays experience a wide spectrum of traveling forces whose spatial distribution consists of an integer number of wavelengths having excitation frequencies equal to an integer multiple of the engine's rotation speed [4]. Such time-varying forces are caused by the non-uniform gas flow interacting with the blades. For stator assemblies as in the case of vane segments arrays, EO traveling waves are no exceptions, but other sources of excitation having mechanical nature might occur. Being directly connected to the engine's casing, the vane segments are known to suffer either 1x or 2x radial vibrations caused by the unbalance at the bearing supporting the rotating shaft [5].

As in the case of turbine bladed disks assemblies where damping is produced by friction phenomena occurring at the specific blade's locations (blade root, shroud, part span shroud) [7, 8] or by adding extra devices (underplatform dampers, snubber) [9, 10, 11, 12], friction damping at the interlocking and hooks joints are proved to be effective to lower vibrations amplitude in stator vane segments arrays [5].

2

The high interest of the scientific community in modeling friction contact at the interfaces between components and its effects on the dynamics of structures is proven by recent academic studies and industrial applications [13, 14, 15]. In this regard, the commonest approach would require finite element (FE) models of components having compatible meshes at the contact interfaces. This condition ensures to use classic node-to-node contact elements based on the Coulomb friction law. Contact forces can therefore be easily evaluated at the interface between components and the non-linear forced response of the structure be predicted. However, such approach just suites mechanical applications where small contact regions are involved. Instead, for problem involving large contact interfaces with highly refined meshes the contact forces evaluation for each pair of nodes would require large computational costs [16, 17].

The drawback of simulating the contact interaction on regions with a high density of nodes can be overcome by employing a solution strategy involving interface reduction methods [18, 19, 20, 21]. These methods usually follow reduction schemes in the class of *Component Mode Synthesis* (CMS), aiming at reducing the dynamics of a structure to few master degrees-of-freedom (DoFs). For non-linear dynamic analyses involving contact the set of master DoFs has to include the physical DoFs where the non-linear contact forces act. When the number of contact DoFs is a significant percentage of the total number of DoFs, the application of common CMS methods loses its efficiency. Interface reduction methods are therefore used to further reduce the number of contact DoFs in order to make the evaluation of the non-linear forced response faster [23].

In this research one of the latest and promising interface reduction method, i.e. the *Gram-Schmidt Interface* (GSI) method [22], is employed to predict in efficient way the non-linearities due to friction at the hook joints and their effect on the forced response of a stator vane segment. In particular, it will be shown how the GSI method is exploited to handle with the huge number of contact DoFs in order to evaluate the forced responses of the system that otherwise would be expensive to predict from a computational point of view.

3

The goodness of the proposed methodology is quantified both in terms of accuracy of the solution and time costs savings on the calculation of non-linear forced responses by comparison with benchmark results obtained by the Poli-contact software [24]. Deeper considerations will be finally carried out on the convenience of properly design the hook joints in order to extend the engine components' life improving the safety margins.

2. THE STATOR VANE SEGMENT

A typical example of a real stator vane segment is shown in Figure 1. This represents the fundamental 'sector' of a stator wheel located in between two subsequent rotor stages. Each vane segment usually exhibits three lap joints through which the interaction with the neighbors components occurs:

- *interlocking joint*: located at the inner radius of the sector it allows the coupling of neighboring segments. When all the segments are assembled resulting in a full stator wheel, the design interference at the interlocking guarantees a certain level of normal preload. During vibration friction onset causes energy dissipation, which is responsible of a response amplitude decrease in resonance conditions.

- *hook joints*: located at the outer radius of the sector, these allow the assembly of each segment to the casing (Figure 2). Being lap joints, hooks are affected by friction during vibration. As in the case of the interlocking these must be considered possible sources of friction damping.
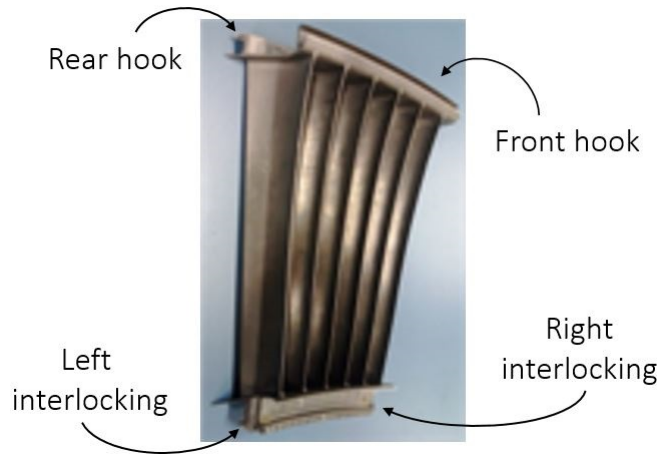

Figure 1: Example of a real vane segment of a low pressure turbine module for aeronatical applications. Courtesy of GE Avio.
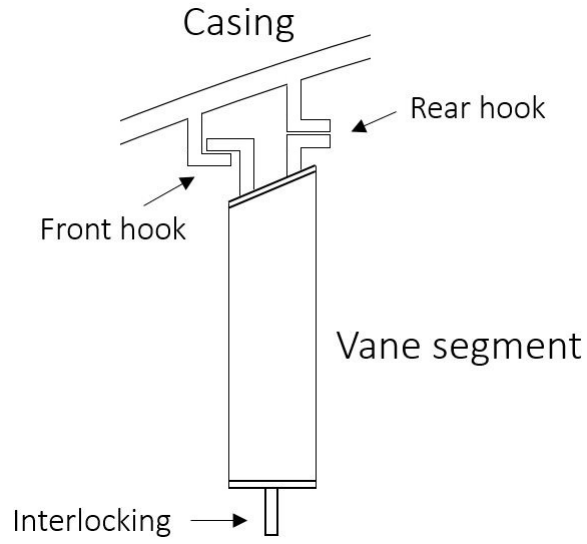
Figure 2: Scheme of a stator vane segment connected at the casing by means of hook joints.

In this research the forced response of a stator wheel is obtained by assuming a traveling wave EO excitation resulting from the action of the unsteady pressure distribution on the blades. Due to the cyclic geometry of the full stator wheel, the vane segment is studied assuming the hypothesis of cyclic symmetry.

3. COMPONENT MODELING AND MATHEMATICAL BACKGROUND

The prediction of the forced response of a structure with friction contacts is a non-linear problem. This is usually solved in the frequency domain by using iterative methods. Depending on the number of DoFs involved in the equations of motion (EQM), iterative methods might require a considerable amount of time to find the optimal solution. A reduction of the number of DoFs is therefore necessary to obtain a reduced order model (ROM) that is able to accurately capture the dynamics of the system by guaranteeing time cost savings as well.

The ROM of the analyzed component is obtained starting from the FE model of a stator vane segment assembled to the corresponding sector of casing. The FE models are connected one to the other by enforcing the compatibility of nodal displacements at the locations where actually the vane segment is prevented from rigid body motion when assembled to the casing.

In this section the reduction process employed to create the ROM is summarized. In particular, more emphasis will be given to the GSI method since it is crucial for the objective of this research. Furthermore, the numerical approach adopted to solve the non-linear reduced EQM of the vane segment in cyclic symmetry condition is discussed.

3.1. TRAN METHOD

Modeling real vane segments requires creating FE models having many thousands of DoFs. For cyclic symmetric structures the method developed by Tran [25] can be used to condense the model dynamics on a highly reduced set of physical DoFs. The first step towards the complete model order reduction is the application of the *Craig-Bampton* CMS (CB-CMS) method based on the following coordinate transformation [26]:

$$\mathbf{x} = \begin{Bmatrix} \mathbf{x}_m \\ \mathbf{x}_s \end{Bmatrix} \approx \begin{bmatrix} \mathbf{I}_{mm} & \mathbf{0}_{mk} \\ \Psi_{sm} & \Phi_{sk} \end{bmatrix} \begin{Bmatrix} \mathbf{x}_m \\ \eta_k \end{Bmatrix} = \mathbf{R}_{CB}\mathbf{x}_{CB} \qquad (1)$$

7

where $\mathbf{x}_m$ and $\mathbf{x}_s$ are the set of *master* and *slave* DoFs, $[\mathbf{I}_{mm}^T \ \Psi_{sm}^T]^T$ is the matrix of constraint modes, while $[\mathbf{0}_{mk}^T \ \Phi_{sk}^T]^T$ is a reduced set of fixed interface normal modes (with $n_k \ll n_s$). The set of master DoFs $\mathbf{x}_m = [\mathbf{x}_{h_v}^T \ \mathbf{x}_{h_c}^T \ \mathbf{x}_i^T \ \mathbf{x}_a^T \ \mathbf{x}_{c_l}^T \ \mathbf{x}_{c_r}^T]^T$ consists of the following set of DoFs:

- $\mathbf{x}_{h_v}$ and $\mathbf{x}_{h_c}$: vector of contact DoFs at the hook joints at the vane and casing side respectively. The numbers of DoFs of these set are denoted by n_h $(dim(\mathbf{x}_{h_v}) = dim(\mathbf{x}_{h_c}) = n_h \times 1)$;

- $\mathbf{x}_i$: vector of contact DoFs at the interlocking joint $(dim(\mathbf{x}_i) = n_i \times 1)$;

- $\mathbf{x}_a$: vector of active DoFs, i.e. DoFs where the response is monitored $(dim(\mathbf{x}_a) = n_a \times 1)$;

- $\mathbf{x}_{c_l}$ and $\mathbf{x}_{c_r}$: DoFs at the left and right casing's frontiers for the application of cyclic symmetry constraints. A good practice would suggest having both sets with the same number of DoFs $(dim(\mathbf{x}_{c_l}) = dim(\mathbf{x}_{c_r}) = n_c \times 1)$.

When the transformation of Eqn. 1 is applied to the FE mass and stiffness matrices $\mathbf{M}$ and $\mathbf{K}$, the corresponding CB-CMS matrices are obtained as follows [26]:

$$\mathbf{M}_{CB} = \mathbf{R}_{CB}^T \mathbf{M} \mathbf{R}_{CB} \qquad \mathbf{K}_{CB} = \mathbf{R}_{CB}^T \mathbf{K} \mathbf{R}_{CB} \tag{2}$$

Cyclic symmetric structures typically show a traveling response characterized by waveforms under the action of a traveling wave EO excitation. The number of waves equals the number of nodal diameters h of the excited mode shape. The consequence is a phase delay φ_h in the motion between the left and right sector's boundaries. This can be mathematically enforced as follows:

$$\mathbf{x}_r = \mathbf{x}_l e^{\iota \varphi_h} \tag{3}$$

By applying the cyclic symmetry constraints of Eqn. 3 between the left and

8

right casing's boundaries $\mathbf{x}_{c_l}$ and $\mathbf{x}_{c_r}$, the vector $\mathbf{x}_{CB}$ becomes:

$$\mathbf{x}_{CB} = \left\{ \begin{array}{c} \mathbf{x}_m \\ \mathbf{q}_k \end{array} \right\} = \left\{ \begin{array}{c} \mathbf{x}_{h_v} \\ \mathbf{x}_{h_c} \\ \mathbf{x}_i \\ \mathbf{x}_a \\ \mathbf{x}_{c_l} \\ \mathbf{x}_{c_r} \\ \mathbf{q}_k \end{array} \right\} = \begin{bmatrix} \mathbf{I} & \mathbf{0} & \mathbf{0} & \mathbf{0} & \mathbf{0} & \mathbf{0} \\ \mathbf{0} & \mathbf{I} & \mathbf{0} & \mathbf{0} & \mathbf{0} & \mathbf{0} \\ \mathbf{0} & \mathbf{0} & \mathbf{I} & \mathbf{0} & \mathbf{0} & \mathbf{0} \\ \mathbf{0} & \mathbf{0} & \mathbf{0} & \mathbf{I} & \mathbf{0} & \mathbf{0} \\ \mathbf{0} & \mathbf{0} & \mathbf{0} & \mathbf{0} & \mathbf{I} & \mathbf{0} \\ \mathbf{0} & \mathbf{0} & \mathbf{0} & \mathbf{0} & \mathbf{I}e^{\iota\varphi_h} & \mathbf{0} \\ \mathbf{0} & \mathbf{0} & \mathbf{0} & \mathbf{0} & \mathbf{0} & \mathbf{I} \end{bmatrix} \left\{ \begin{array}{c} \mathbf{x}_{h_v}^{cs} \\ \mathbf{x}_{h_c}^{cs} \\ \mathbf{x}_i^{cs} \\ \mathbf{x}_a^{cs} \\ \mathbf{x}_{c_l}^{cs} \\ \mathbf{q}_k^{cs} \end{array} \right\} \tag{4}$$

A Guyan ROM is created from the FE model by just retaining as master the sets of DoFs $\mathbf{x}_{c_l}$ and $\mathbf{x}_{c_r}$. By grouping such sets into the vector $\mathbf{x}_c = [\mathbf{x}_{c_l}^T \ \mathbf{x}_{c_r}^T]^T$, the following coordinate transformation holds:

$$\mathbf{x} = \left\{ \begin{array}{c} \mathbf{x}_c \\ \mathbf{x}_s \end{array} \right\} \approx \begin{bmatrix} \mathbf{I}_{cc} \\ \Psi_{sc} \end{bmatrix} \mathbf{x}_c \tag{5}$$

where $\mathbf{x}_s$ is the vector of remaining slave DoFs and $[\mathbf{I}_{cc}^T \ \Psi_{sc}^T]^T$ is the matrix collecting the $2 \times n_c$ constraint modes. Then, $\mathbf{x}_{c_r}$ is expressed in terms of $\mathbf{x}_{c_l}$ by employing the same cyclic constraints of Eqn. 4:

$$\mathbf{x}_c = \left\{ \begin{array}{c} \mathbf{x}_{c_l} \\ \mathbf{x}_{c_r} \end{array} \right\} = \begin{bmatrix} \mathbf{I} \\ \mathbf{I}e^{i\varphi_h} \end{bmatrix} \mathbf{x}_{c_l}^h = \mathbf{R}_{G_{cs}} \mathbf{x}_{c_l}^{cs} \tag{6}$$

By projecting the Guyan EQM onto the basis $\mathbf{R}_G^{cs}$, the following EQM are obtained:

$$\mathbf{M}_G^{cs} \ \ddot{\mathbf{x}}_{c_l}^{cs} + \mathbf{K}_G^{cs} \ \mathbf{x}_{c_l}^{cs} = \mathbf{0} \tag{7}$$

where

$$\mathbf{M}_G^{cs} = (\mathbf{R}_G^{cs})^* \mathbf{M}_G \mathbf{R}_G^{cs} \qquad \mathbf{K}_G^{cs} = (\mathbf{R}_G^{cs})^* \mathbf{K}_G \mathbf{R}_G^{cs} \tag{8}$$

According to the Tran method [25] the motion at the left frontier DoFs $\mathbf{x}_{c_l}^{cs}$ can be approximated by few eigenvectors of the following eigenproblem:

$$\left(\mathbf{K}_G^{cs} - \omega_j^2 \mathbf{M}_G^{cs} \right) \phi_j^{cs} = \mathbf{0} \qquad \forall \ j = 1, \dots, n_c \tag{9}$$

9

If a subset of n_u eigenvectors is arranged as the columns of a matrix $\Phi_{c_u}^{cs}$, the CB-CMS DoFs vector in cyclic symmetry conditions becomes:

$$\mathbf{x}_{CB}^{cs} = \begin{Bmatrix} \mathbf{x}_{h_v}^{cs} \\ \mathbf{x}_{h_c}^{cs} \\ \mathbf{x}_i^{cs} \\ \mathbf{x}_a^{cs} \\ \mathbf{x}_{c_l}^{cs} \\ \mathbf{q}_k^{cs} \end{Bmatrix} \approx \begin{bmatrix} \mathbf{I} & \mathbf{0} & \mathbf{0} & \mathbf{0} & \mathbf{0} & \mathbf{0} \\ \mathbf{0} & \mathbf{I} & \mathbf{0} & \mathbf{0} & \mathbf{0} & \mathbf{0} \\ \mathbf{0} & \mathbf{0} & \mathbf{I} & \mathbf{0} & \mathbf{0} & \mathbf{0} \\ \mathbf{0} & \mathbf{0} & \mathbf{0} & \mathbf{I} & \mathbf{0} & \mathbf{0} \\ \mathbf{0} & \mathbf{0} & \mathbf{0} & \mathbf{0} & \Phi_{c_u}^{cs} & \mathbf{0} \\ \mathbf{0} & \mathbf{0} & \mathbf{0} & \mathbf{0} & \mathbf{0} & \mathbf{I} \end{bmatrix} \begin{Bmatrix} \mathbf{x}_{h_v}^{cs} \\ \mathbf{x}_{h_c}^{cs} \\ \mathbf{x}_i^{cs} \\ \mathbf{x}_a^{cs} \\ \mathbf{q}_u^{cs} \\ \mathbf{q}_k^{cs} \end{Bmatrix} \qquad (10)$$

The coordinate transformation of Eqn. 10 is clearly effective if $n_u \ll n_c$. Henceforth the superscript cs referring to the cyclic symmetric quantities will be omitted in order to simplify the notation.

3.2. GSI REDUCTION METHOD

The GSI reduction method is an upgrade of the pre-existing technique based on the Characteristic Constraint Modes (CC modes) [18]. Similarly to the classic CMS methods, the GSI technique allows for the reduction of a subset of master DoFs by truncating a basis of modes known as GSI modes [22]. In this study the GSI method is applied to the ROM of Eqn.10. By grouping the physical and modal DoFs as follows:

$$\mathbf{x}_m = \begin{Bmatrix} \mathbf{x}_{h_v} \\ \mathbf{x}_{h_c} \\ \mathbf{x}_i \\ \mathbf{x}_a \end{Bmatrix} \quad \text{and} \quad \mathbf{q}_t = \begin{Bmatrix} \mathbf{q}_u \\ \mathbf{q}_k \end{Bmatrix} \tag{11}$$

the EQM become:

$$\begin{bmatrix} \mathbf{M}_{mm} & \mathbf{M}_{mt} \\ \mathbf{M}_{tm} & \mathbf{M}_{tt} \end{bmatrix} \begin{Bmatrix} \ddot{\mathbf{x}}_m \\ \ddot{\mathbf{q}}_t \end{Bmatrix} + \begin{bmatrix} \mathbf{K}_{mm} & \mathbf{K}_{mt} \\ \mathbf{K}_{tm} & \mathbf{K}_{tt} \end{bmatrix} \begin{Bmatrix} \mathbf{x}_m \\ \mathbf{q}_t \end{Bmatrix} = \begin{Bmatrix} \mathbf{f}_m \\ \phi_t \end{Bmatrix} \tag{12}$$

where the quantities identified by the subscript m refer to the physical partition. By solving the eigenproblem defined by $\mathbf{K}_{mm}$ and $\mathbf{M}_{mm}$ the full set of CC modes is obtained. These can be arranged for increasing eigenvalues as the columns of the following modal matrix:

$$\Phi_{mm} = \begin{bmatrix} \varphi_1 & \dots & \varphi_{n_m} \end{bmatrix} \tag{13}$$

The modal matrix of Eqn. 13 would allow for a coordinate transformation involving all the master DoFs. If a coordinate transformation is desired just for a subset of n_p physical DoFs, Φ_{mm} has to be partitioned as follows:

$$\mathbf{x}_m = \begin{Bmatrix} \mathbf{x}_p \\ \mathbf{x}_r \end{Bmatrix} = \Phi_{mm} \begin{Bmatrix} \mathbf{q}_p \\ \mathbf{q}_r \end{Bmatrix} = \begin{bmatrix} \Phi_{pp} & \Phi_{pr} \\ \Phi_{rp} & \Phi_{rr} \end{bmatrix} \begin{Bmatrix} \mathbf{q}_p \\ \mathbf{q}_r \end{Bmatrix} \tag{14}$$

where $\mathbf{q}_p$ and $\mathbf{q}_r$ are two arbitrary set of modal coordinates with size n_p and n_r respectively. Previous studies on the GSI method proved that performing a *Gram-Schmidt* orthonormalization on the columns of Φ_{pp} produces a good reduction basis for the physical partition $\mathbf{x}_p$ [29].

3.3. NON-LINEAR EQUATION OF MOTION

The non-linear reduced EQM of a vane segment with friction contacts can be written as:

$$\mathbf{M}\ddot{\mathbf{x}}(t) + \mathbf{C}\dot{\mathbf{x}}(t) + \mathbf{K}\mathbf{x}(t) = \mathbf{f}_e(t) - \mathbf{f}_{nl}(\mathbf{x}, \dot{\mathbf{x}}, t) \tag{15}$$

where $\mathbf{M}$, $\mathbf{C}$ and $\mathbf{K}$ are the reduced mass, damping and stiffness matrices, $\mathbf{x}$ is the reduced vector of DoFs, $\mathbf{f}_e$ and $\mathbf{f}_{nl}$ the corresponding vectors of the external and non-linear contact forces. When the steady state response is of interest, it is common to solve the former EQM in the frequency domain. Due to the periodicity of $\mathbf{f}_e$, the displacements and non-linear contact forces can be written according to the following Fourier series:

$$\mathbf{x}(t) = \Re\left(\sum_{f=0}^{n_h} \mathbf{X}^{(f)} \cdot e^{if\omega t}\right)$$

$$\mathbf{f}_{nl}(\mathbf{x}, \dot{\mathbf{x}}, t) = \Re\left(\sum_{f=0}^{n_h} \mathbf{F}_{nl}^{(f)} \cdot e^{if\omega t}\right) \tag{16}$$

where $\mathbf{X}^{(f)}$ and $\mathbf{F}_{nl}^{(f)}$ are the fth order complex amplitudes of the displacements and contact forces respectively, ω is the circular frequency and n_h is the number of retained harmonics. The differential equations in Eqn. 15 can then be turned into the following set of non-linear, complex, algebraic equations:

$$\mathbf{D}^{(f)}(\omega)\mathbf{X}^{(f)} = \mathbf{F}_e^{(f)} - \mathbf{F}_{nl}^{(f)}(\mathbf{X}) \qquad \forall\, f = 0, 1, 2, \ldots, n_h \tag{17}$$

where $\mathbf{D}^{(f)} = \mathbf{K} + if\omega\mathbf{C} - (f\omega)^2\mathbf{M}$ is the fth order dynamic stiffness matrix. By assuming the 1st order approximation for $\mathbf{x}$ and $\mathbf{f}_{nl}$ (SHBM approximation), Eqn. 17 can be rewritten as:

$$\mathbf{D}(\omega)\mathbf{X} - \mathbf{F}_e + \mathbf{F}_{nl}(\mathbf{X}) = 0 \tag{18}$$

with the superscript $^{(f)}$ omitted in order to simplify the notation. Note that Eqn. 18 can not be solved analytically due to its non-linear nature. It has to be solved iteratively for the unknown amplitudes $\mathbf{X}$.

12

Without loss of generality, let assume to denote the partitions of the non-linear EQM with superscripts v and c referring to the vane and casing respectively. Moreover, let the number of DoFs at the hooks be the same for the casing and vane's side, i.e. n_h. Under these assumptions, the global mass and stiffness matrices and the vectors of Eqn. 18 can be expressed as:

$$
\mathbf{M} = \begin{bmatrix} \mathbf{M}_{hh}^v & \mathbf{M}_{ho}^v & \mathbf{0} & \mathbf{0} \\ \mathbf{M}_{oh}^v & \mathbf{M}_{oo}^v & \mathbf{0} & \mathbf{0} \\ \mathbf{0} & \mathbf{0} & \mathbf{M}_{hh}^c & \mathbf{M}_{ho}^c \\ \mathbf{0} & \mathbf{0} & \mathbf{M}_{oh}^c & \mathbf{M}_{oo}^c \end{bmatrix} \qquad \mathbf{K} = \begin{bmatrix} \mathbf{K}_{hh}^v & \mathbf{K}_{ho}^v & \mathbf{0} & \mathbf{0} \\ \mathbf{K}_{oh}^v & \mathbf{K}_{oo}^v & \mathbf{0} & \mathbf{0} \\ \mathbf{0} & \mathbf{0} & \mathbf{K}_{hh}^c & \mathbf{K}_{ho}^c \\ \mathbf{0} & \mathbf{0} & \mathbf{K}_{oh}^c & \mathbf{K}_{oo}^c \end{bmatrix}
$$

$$
\mathbf{x} = \begin{Bmatrix} \mathbf{X}_h^v \\ \mathbf{X}_o^v \\ \mathbf{X}_h^c \\ \mathbf{X}_o^c \end{Bmatrix} \qquad \mathbf{f}_e = \begin{Bmatrix} \mathbf{0} \\ \mathbf{F}_{o_e}^v \\ \mathbf{0} \\ \mathbf{0} \end{Bmatrix} \qquad \mathbf{f}_{nl} = \begin{Bmatrix} \mathbf{F}_{h_{nl}}^v \\ \mathbf{0} \\ \mathbf{F}_{h_{nl}}^c \\ \mathbf{0} \end{Bmatrix} \tag{19}
$$

where the subpartitions identified by the subscript h refer to the contact DoFs at the hooks. By looking at the force vectors in the Eqn. 19, it must be pointed out that both the external excitation due to the unsteady pressure distribution $\mathbf{F}_{o_e}^v$ and the contact forces at the interlocking joint are applied to the vane's partition only.

Since $\mathbf{f}_{nl}$ only depends on the relative displacements at the contact interface, the number of non-linear algebraic equations corresponding to the hooks DoFs can be halved by employing the coordinate transformation from absolute to relative interface displacements:

$$
\begin{Bmatrix} \mathbf{X}_h^v \\ \mathbf{X}_o^v \\ \mathbf{X}_h^c \\ \mathbf{X}_o^c \end{Bmatrix} = \begin{bmatrix} \mathbf{I} & \mathbf{I} & \mathbf{0} & \mathbf{0} \\ \mathbf{0} & \mathbf{0} & \mathbf{I} & \mathbf{0} \\ \mathbf{0} & \mathbf{I} & \mathbf{0} & \mathbf{0} \\ \mathbf{0} & \mathbf{0} & \mathbf{0} & \mathbf{I} \end{bmatrix} \begin{Bmatrix} \mathbf{X}_h^{rel} \\ \mathbf{X}_h^c \\ \mathbf{X}_o^v \\ \mathbf{X}_o^c \end{Bmatrix} = \mathbf{R}\mathbf{X}^{rel} \tag{20}
$$

where $\mathbf{X}_h^{rel} = \mathbf{X}_h^v - \mathbf{X}_h^c$ and $\mathbf{R}$ is the coordinate transformation matrix.

By substituting Eqn. 20 into Eqn. 18 and pre-multiplying both sides by $\mathbf{R}^T$, the following system of equations is obtained:

$$\mathbf{R}^T\mathbf{D}\mathbf{R}\mathbf{X}^{rel} - \mathbf{R}^T\mathbf{F}_e + \mathbf{R}^T\mathbf{F}_{nl}(\mathbf{X}^{rel}) \approx 0 \quad \Rightarrow$$

$$\mathbf{D}^{rel}\mathbf{X}^{rel} - \mathbf{F}_e^{rel} + \mathbf{F}_{nl}^{rel}(\mathbf{X}^{rel}) \approx 0 \tag{21}$$

Although the pre-multiplication by $\mathbf{R}$ leaves $\mathbf{F}_e$ unchanged, more attention has to be paid on the term $\mathbf{F}_{nl}^{rel}$:

$$\mathbf{F}_{nl}^{rel} = \mathbf{R}^T\mathbf{F}_{nl} = \begin{bmatrix} \mathbf{I} & \mathbf{0} & \mathbf{0} & \mathbf{0} \\ \mathbf{I} & \mathbf{0} & \mathbf{I} & \mathbf{0} \\ \mathbf{0} & \mathbf{I} & \mathbf{0} & \mathbf{0} \\ \mathbf{0} & \mathbf{0} & \mathbf{0} & \mathbf{I} \end{bmatrix} \begin{Bmatrix} \mathbf{F}_{h_{nl}}^v \\ \mathbf{0} \\ \mathbf{F}_{h_{nl}}^c \\ \mathbf{0} \end{Bmatrix} = \begin{Bmatrix} \mathbf{F}_{h_{nl}}^v \\ \mathbf{F}_{h_{nl}}^c + \mathbf{F}_{h_{nl}}^c \\ \mathbf{0} \\ \mathbf{0} \end{Bmatrix} \tag{22}$$

The forces at the contact interface are equal in amplitude but opposite in sign, meaning that the term $\mathbf{F}_{h_{nl}}^c + \mathbf{F}_{h_{nl}}^c$ is null:

$$\mathbf{R}^T\mathbf{f}_{nl} = \begin{bmatrix} \mathbf{I} & \mathbf{0} & \mathbf{0} & \mathbf{0} \\ \mathbf{I} & \mathbf{0} & \mathbf{I} & \mathbf{0} \\ \mathbf{0} & \mathbf{I} & \mathbf{0} & \mathbf{0} \\ \mathbf{0} & \mathbf{0} & \mathbf{0} & \mathbf{I} \end{bmatrix} \begin{Bmatrix} \mathbf{F}_{h_{nl}}^v \\ \mathbf{0} \\ \mathbf{F}_{h_{nl}}^c \\ \mathbf{0} \end{Bmatrix} = \begin{Bmatrix} \mathbf{F}_{h_{nl}}^v \\ \mathbf{0} \\ \mathbf{0} \\ \mathbf{0} \end{Bmatrix} \tag{23}$$

In this way the number of non-linear EQM describing the contact state at the hooks can be finally decreased from $2 \times n_h$ to n_h.

Due to the large extension of the contact interfaces at the hooks, a further reduction can be achieved by employing the GSI method. If Φ_{hw} is a reduced basis with $n_w \ll n_h$ GSI modes, the vector of complex relative displacements $\mathbf{X}^{rel}$ can be expressed as:

$$\mathbf{X}^{rel} = \begin{Bmatrix} \mathbf{X}_h^{rel} \\ \mathbf{X}_h^c \\ \mathbf{X}_o^v \\ \mathbf{X}_o^c \end{Bmatrix} \approx \begin{bmatrix} \Phi_{iw} & \mathbf{0} & \mathbf{0} & \mathbf{0} \\ \mathbf{0} & \mathbf{I} & \mathbf{0} & \mathbf{0} \\ \mathbf{0} & \mathbf{0} & \mathbf{I} & \mathbf{0} \\ \mathbf{0} & \mathbf{0} & \mathbf{0} & \mathbf{I} \end{bmatrix} \begin{Bmatrix} \mathbf{Q}_w^{rel} \\ \mathbf{X}_h^c \\ \mathbf{X}_o^v \\ \mathbf{X}_o^c \end{Bmatrix} = \mathbf{G}\mathbf{X}_{GSI}^{rel} \tag{24}$$

14

where $\mathbf{Q}_w^{rel}$ is the complex amplitudes vector of the modal coordinates $\mathbf{q}_{hw}$. By projecting the Eqn. 20 onto the space spanned by the columns of $\mathbf{G}$, the following relationship is obtained:

$$\mathbf{G}^T \mathbf{D}^{rel} \mathbf{G} \mathbf{X}_{GSI}^{rel} - \mathbf{G}^T \mathbf{F}_e^{rel} + \mathbf{G}^T \mathbf{F}_{nl}^{rel}(\mathbf{X}_{GSI}^{rel}) \approx 0 \qquad (25)$$

with:

$$\mathbf{G}^T \mathbf{F}_{nl}^{rel} = \begin{Bmatrix} \Phi_{iw} \mathbf{F}_{h_{nl}}^v \\ \mathbf{0} \\ \mathbf{0} \\ \mathbf{0} \end{Bmatrix} \qquad (26)$$

where the term $\Phi_{iw} \mathbf{F}_{nl_h}^v$ represents the vector of the modal contact forces. Although the contact forces $\mathbf{F}_{nl_h}$ are always estimated in the space of the physical DoFs, these are introduced into the EQM in a reduced like form by means of the modal coordinates $\mathbf{q}_w^{rel}$. This procedure allows for a faster solution of the non-linear partition of Eqn 24, that otherwise would be computationally expensive as in the case of Eqn. 18.

The strategy used to build the reduced basis of Φ_{iw} is later discussed in section 4, since it strictly depends on the physics behind the contact phenomena occurring at the hooks.

3.4. CONTACT MODEL

The one-dimensional Jenkins contact element with normal load variation is used to compute the periodic contact forces for a given periodic relative displacement, by taking into account possible separation of the contact interfaces [6]. The Jenkins contact element models three different contact states: stick, slip and separation. A schematic view of this contact model can be found in Figure 3, where the two dimensional relative displacement is decomposed into two perpendicular directions: two in-plane tangential component denoted by the u and w components, and one out-of-plane normal component v.
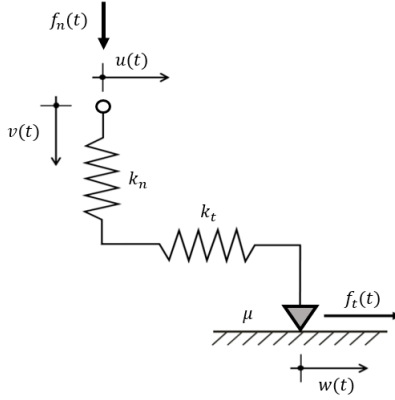
Figure 3: 1-D contact model with normal load variation.

The contact model's parameters are represented by the tangential and normal contact stiffnesses, k_t and k_n respectively, the coefficient of friction μ and the normal preload f_o (see Figure 3). At every time instant the normal contact force $f_n(t)$ is defined as:

$$f_n = \max(f_o + k_n \cdot v, 0) \qquad (27)$$

If f_o is positive, the bodies are in contact before vibration starts, while if f_o is negative an initial gap $g_o = -\frac{f_o}{k_n}$ exists between the two bodies.

16

Along the tangential direction, the contact force is defined as:

$$
f_t = \begin{cases} k_t \cdot (u - w) & \text{sticking mode} \\ \operatorname{sgn}(\dot{w}) \cdot \mu f_n & \text{slipping mode} \\ 0 & \text{lift-off mode} \end{cases} \tag{28}
$$

Since the EQM are expressed in the frequency domain, the Fourier coefficients of the non-linear contact forces $\mathbf{F}^v_{h_{nl}}$ have to be computed from the Fourier coefficients of the corresponding relative displacement $\mathbf{X}^{rel}$. This is done by using the *Alternating Frequency Time* (AFT) method [27, 28]. Basically, the Fourier coefficients of the displacements are used to reconstruct the corresponding quantity in the time domain by means of the inverse Fourier transform. These are used as inputs to the contact model in order to compute the physical contact forces. Finally, the contact forces Fourier coefficients are evaluated by Fast Fourier Transform (FFT) and introduced into Eqn 17.

4. METHOD APPLICATION

The reduction method introduced in section 3 is here applied to a FE model consisting of a stator vane segment connected to a casing sector. According to the DoFs partitions a preliminary CB-CMS ROM was created by retaining as master the following sets of DoFs (Figure 4):

- $n_{h_v} = n_{h_c} = n_h = 450$ DoFs at the hooks for the vane and casing. These sets DoFs are spread over the hooks as shown in Figure 4.

- $n_i = 144$ DoFs at the interlocking joint. n_i includes both the contact DoFs at the left and right vane's interlocking.

- $n_a = 72$ DoFs at the vane's blade and casing's outer surface;

- $n_c = 3080$ DoFs at the left and right casing frontiers for the application of cyclic symmetry constraints.

- $n_k = 100$ modal coordinates corresponding to the reduced basis of fixed interface normal modes retained in the reduction.

Furthermore, by applying the Tran method combined with cyclic symmetry constraints for a harmonic index 2, the DoFs partitions $\mathbf{x}_{c_l}$ and $\mathbf{x}_{c_r}$ are reduced with $n_u = 100$ interface modal coordinates. The obtained ROM is such that mode shapes and natural frequencies of the starting FE model are captured with high accuracy (maximum percentage error on the natural frequencies $< 0.1\%$).
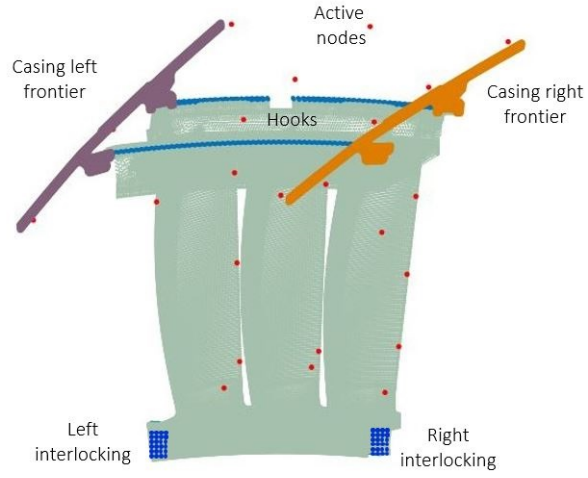
Figure 4: Master nodes retained in the CB-CMS ROM.

The reduction of the hooks DoFs by the GSI method requires further considerations. Depending on the nature of the external excitation, the preload and the contact parameters, the system's response usually follows the typical trend of the slip-stick non-linear phenomenon (Figure 5).
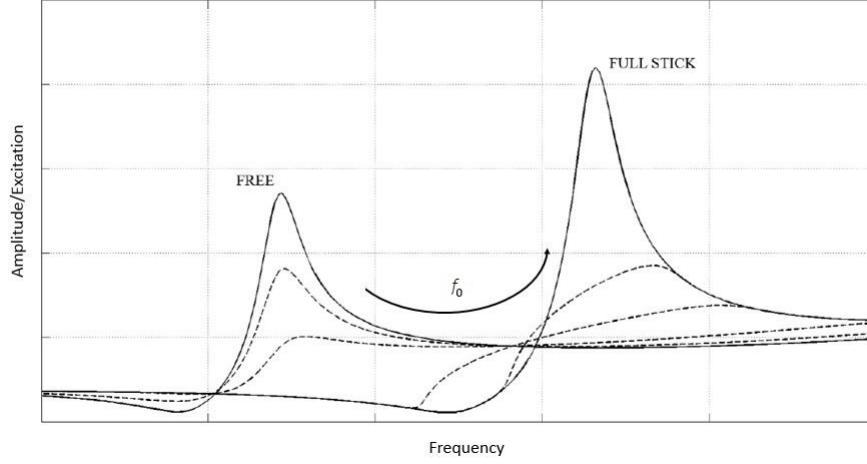
19

Figure 5: Stick-slip phenomenon in the frequency domain: an increase of the preload f_0 at the hooks has the effect of shifting the resonant frequency towards higher values, moving from the *free* to the *full-stick* configuration.

For a certain amplitude of the aerodynamic excitation and prescribed value of the preload at the interlocking, an increase of the preload at the hooks has the effect of shifting the resonant frequency towards higher values, moving from the *free* configuration (i.e. no contact occurs during the whole vibration cycle) to the *full-stick* configuration. It is also quite crucial understanding the nature of the structure's mode shapes for these two extreme configurations. In the free case the relative displacement at the hooks is so large that friction is ineffective in damping the system response. In the fully stick case the structure behaves as if it were fully assembled since small relative displacements at the contact interface occur. According to these observations, the motion at the hooks has to be described with a basis of GSI modes that is representative of both the free and full-stick conditions at the contact interfaces. Such basis is here obtained by applying the mathematical procedure described in section 3 on two sets of linear matrices:

- the free matrices, $\mathbf{M}_{fr}^{rel}$ and $\mathbf{K}_{fr}^{rel}$, obtained by just applying the coordinate transformation of Eqn. 20 to the mass and stiffness matrix of Eqn. 19;

20

- the full-stick matrices, $\mathbf{M}_{fs}^{rel}$ and $\mathbf{K}_{fs}^{rel}$, defined as:

$$\mathbf{M}_{fs}^{rel} = \mathbf{M}_{fr}^{rel} \qquad \begin{cases} \mathbf{K}_{fs}^{rel} = \mathbf{R}^T \mathbf{K}_{fs} \mathbf{R} \\[2mm] \mathbf{K}_{fs} = \mathbf{K}_{fr} + \mathbf{K}_{link} \end{cases} \tag{29}$$

where $\mathbf{K}_{link}$ performs the assembly of the hooks nodes belonging to the vane and casing by means of a set of node-to-node springs having the same stiffness assumed for the contact elements. If the matrix $\mathbf{K}_{fr}$ is partitioned as in Figure 6 a), the structure of $\mathbf{K}_{link}$ is that of Figure 6 b). $\mathbf{K}_{link}$ collects the elementary stiffness sub-matrices including the spring elements that are used to link the DoFs at the vane's hooks to the corresponding casing's ones.
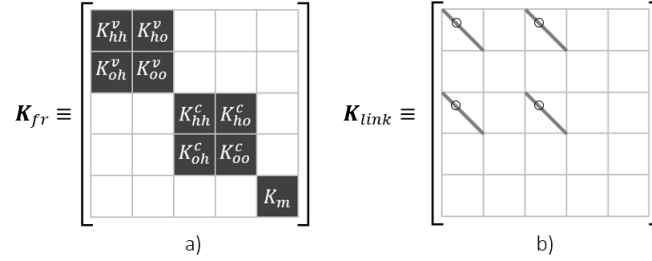
Figure 6: $\mathbf{K}_{fr}$ partitions used to solve the current dynamical system a) and $\mathbf{K}_{link}$ structure b). The m subscript identify the partition corresponding to the modal coordinates, while all the other subscripts have the meanings already defined in section 3.3.

In detail, the four circled locations highlighted in the matrix of Figure 6 b) accommodate the four coefficients of the elementary stiffness matrix $\mathbf{K}_e$ defined as:

$$\mathbf{K}_e = \begin{bmatrix} k_e & -k_e \\ -k_e & k_e \end{bmatrix} \tag{30}$$

where:

- $k_e = k_t$ if the spring connects two DoFs acting along a direction which is tangential to the contact surface;

- $k_e = k_n$ if the spring connects two DoFs acting along a direction which is normal to the contact surface.

21

The results of the assembly procedure leading to the full-stick model can be finally visualized in Figure 7.

Figure 7: Assembly procedure for the CB-CMS stiffness matrices: the K_{link} matrix links the corresponding contact nodes at the hooks by local contact stiffnesses in the tangential and normal directions.

In this way two bases of GSI modes are obtained (Φ_{hh}^{fr} and Φ_{hh}^{fs} corresponding to the free and full-stick models of Figure 8) and the reduction of the relative interface DoFs finally performed.
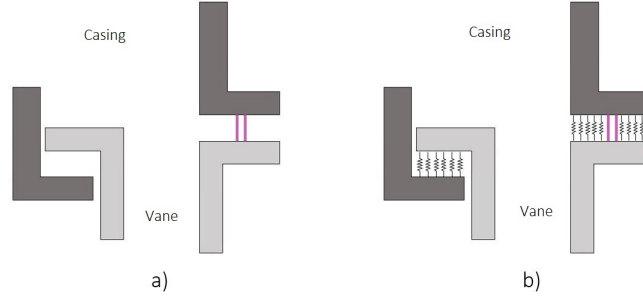

Figure 8: Hooks in the free configuration a), hooks in the full-stick configuration b).

In this research the strategy adopted to accomplish the mentioned task is based on the definition of a reduction basis collecting $n_w \ll n_h$ GSI modes from the bases Φ_{hh}^{fr} and Φ_{hh}^{fs}:

$$\Phi_{hw} = \left[\Phi_{hw_{fr}}^{fr} \ \Phi_{hw_{fs}}^{fs} \right] \tag{31}$$

with the subscript w_{fr} and w_{fs} denoting the number of GSI modes retained from each basis, i.e. $n_{w_{fr}}$ and $n_{w_{fs}}$ for Φ_{hh}^{fr} and Φ_{hh}^{fs} respectively. The choice

22

on the numbers $n_{w_{f_r}}$ and $n_{w_{f_s}}$ is discussed in the application presented in the following section.

4.1. REDUCTION OF THE HOOK INTERFACES

205   In order to test the performances of the GSI method, a set of benchmark frequency response functions (FRFs) was evaluated by means of the *Policontact* software [24]. Computing the FRFs required the definition of a structural damping matrix, which was built by calculating eigenvalues and eigenvectors of the corresponding dynamic system and assuming a modal damping ratio ζ

210 for all the modes. The reduced damping matrix was finally calculated by the inverse transformation to the physical domain using the inverse of the modal matrix [17]. In order to evaluate the friction forces for each pair of nodes in contact, two 1-D Jenkins contact elements with normal load variation acting along two orthogonal directions on the contact plane were used. The contact

215 parameters used to run the numerical simulations, i.e. friction coefficient, contact stiffnesses and design preloads, were provided by GE Avio. For validation purposes the normal preload at the interlocking was chosen in order to prevent any friction phenomena at the interlocking itself. The same value of preload at the interlocking was assumed for all the benchmark FRFs. The sensitivity

220 parameter for the FRFs is just represented by the normal preload F_{0_h}, which was assumed equal for the front and rear hook. Figure 9 shows the trend of the FRFs by varying F_{0_h}. As expected, decreasing the value of F_{0_h} makes the hooks increasingly lose. This results in larger relative displacements at the contact interface, which causes energy dissipation by friction and a consequent reduction

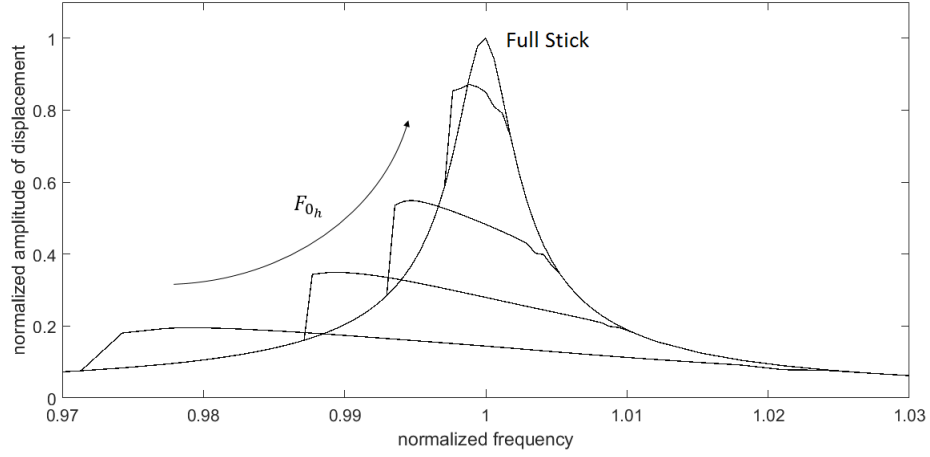225 of the vane vibration amplitude.

Figure 9: Benchmark FRFs obtained by varying the preload F_{0_h} at the hook joint.

In Figure 10 the non-linear FRFs evaluated by using the GSI reduction method are compared with the benchmark calculations of Figure 9. From the
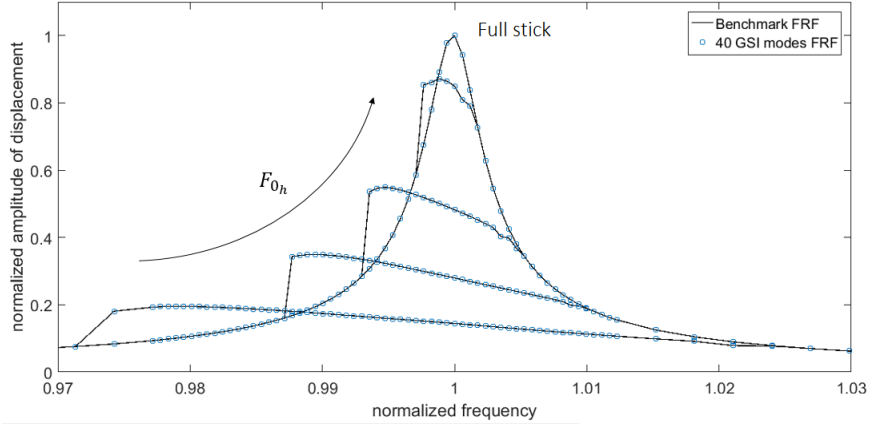

Figure 10: Comparison between the benchmark FRFs of Figure 9 and the FRFs obtained reducing the hooks interfaces with 40 GSI modes.

previous figure it can be noted that reducing the hooks interfaces with 40 GSI modes, i.e. 20 computed with the system in free conditions and 20 with the system in full-stick conditions, ensures a perfect correspondence with the benchmark FRFs. In particular, no significant differences can be found in the FRFs

25

neither in terms of vibration amplitude nor in terms of resonance frequency even if light jumps occur (Figure 10)[1].

The best performance of the GSI reduced model can be easily justified in terms of the size of the model (1316 DoFs of the ROM without GSI reduction vs 436 DoFs of the GSI ROM) and time spent in the computation of each non-linear forced response (i.e. the calculation performed with the non-reduced contact interface is ∼300 times slower than the calculation performed after the application of the GSI reduction technique). Note that the GSI reduction is particularly effective on the non-linear partition of the EQM corresponding to the hooks DoFs, whose size decreases from 900 to 40. This difference strongly decrease the computational costs for the solution of the non-linear partition of the dynamic problem.

Computational times can be further decreased when using a basis with 20 GSI modes (10 in free conditions and 10 in full-stick conditions). (Figure 11). In this case, although the response prediction remains acceptable, the goodness of the previous approximation is partially lost.
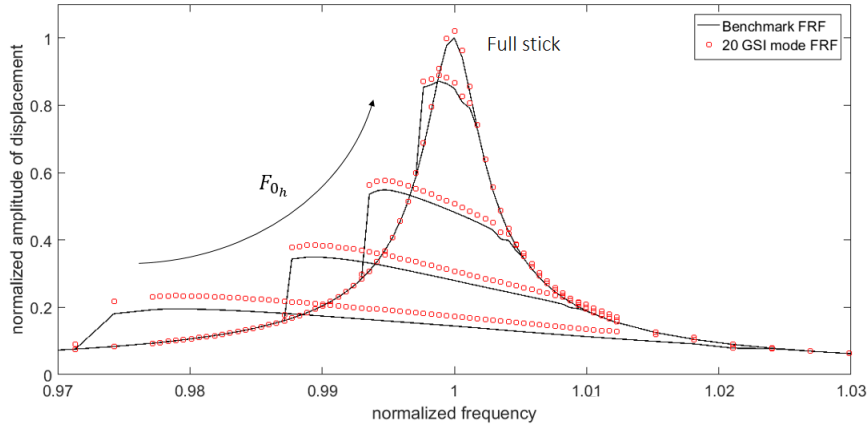

Figure 11: Comparison between the benchmark FRFs of Figure 9 and the FRFs obtained reducing the hooks interfaces with 20 GSI modes.

---

[1]Further details on the accuracy of the GSI method for the prediction of non-linear forced responses in the presence of jump phenomenon can be found in [23].

4.2. DAMPING CAPABILITY OF THE HOOK JOINT

The results of the sensitivity analysis performed in the previous section can be exploited in order to investigate in an efficient way the damping capability of the two joints together (hooks and interlocking). For this reason two conditions are here analyzed. First, the effect of the interlocking joint, preloaded with a design value $F_{0_i}^d$ of the normal load, is assessed on the system response when full-stick state is present at both hooks. Second, for the same $F_{0_i}^d$, the additional damping capability of the hooks is evaluated. In this case the values of the preload at the hooks depends on the amplitude of the steady pressure distribution acting on the stator blades. In both cases the motion of the DoFs at the hooks is still approximated with a set of 40 GSI.
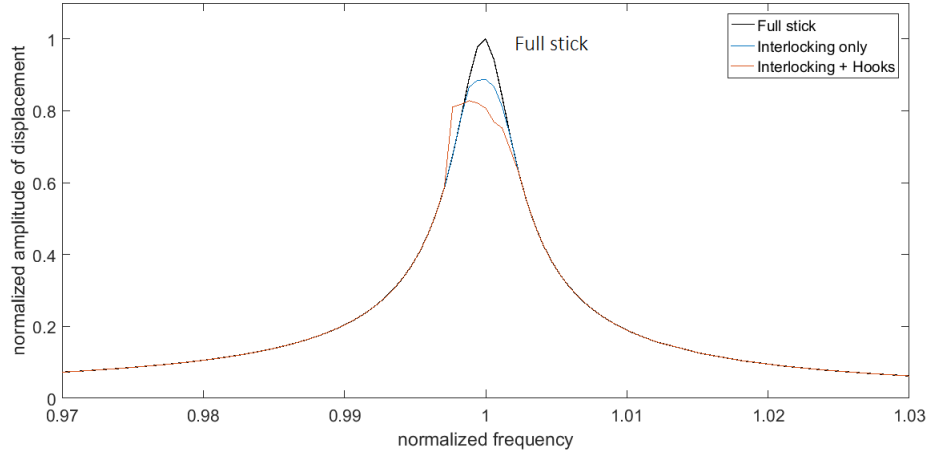

Figure 12: FRFs obtained for sliding interlocking and stuck hooks (blue plot) and both joints sliding (interlocking and hooks, orange plot).

Figure 12 shows the comparison of the FRFs corresponding to the mentioned cases. From the first case (blue curve) it can be noted that a proper design of the interlocking might allows for a significant reduction ($\sim 10\%$) of the system response. By letting both joints slip (red curve) a further 5% decrease in the peak vibration amplitude occurs. Figure 13 shows the percentages of energy dissipation at resonance caused by friction at the interlocking and hooks joints.
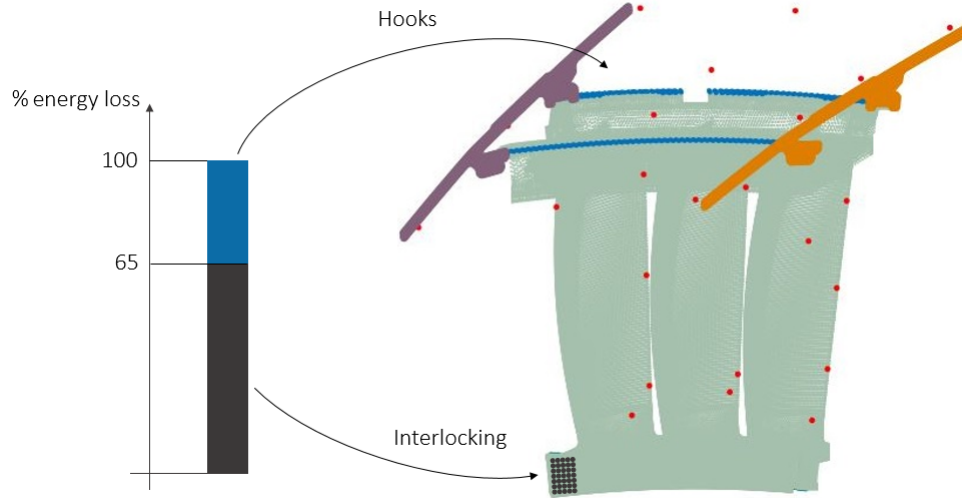
27

Figure 13: Percentages of energy loss by friction associated to the interlocking and hooks joints.

In accordance to the FRFs of Figure 12, the histogram of Figure 13 suggests higher effectiveness of the interlocking with respect the hooks in damping vibrations (65% vs 35% of energy loss by friction). This behavior is due to the different looseness of the joints resulting in a different amount of slip. A deeper investigation of the contact state at the interfaces gives further insights on the interpretation of the FRFs. In particular, Figure 14 schematize the contact state at the rear and front hooks in resonance conditions. Both hooks show a symmetric contact state, which surely depends on the applied cyclic symmetry boundary conditions at the casing (the left and right casing's frontiers vibrate with a phase lag but the same amplitude). In particular, stick-slip occurs everywhere except for the region where compatibility conditions of nodal displacements were enforced before performing the CB-CMS reduction (circled locations at the anti-rotation slot). However, not all the regions are equally effective in damping vibration energy by friction. This is due to the different amount of relative displacement that is influenced by the presence of the anti-rotation slot. The integral of dissipated energy at all the hooks regions was
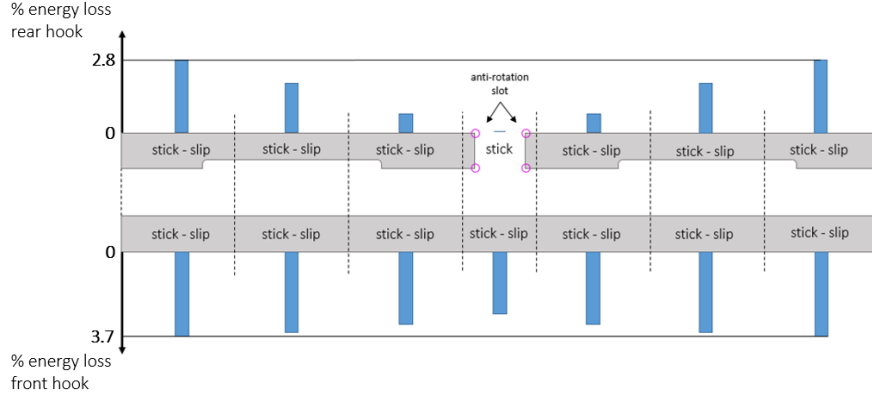
28

Figure 14: Contact state at the hooks in resonance conditions and the percentages of dissipated energy at seven discrete regions along the joints. Each blue bar represents the average percentage of dissipated energy at each region.

quantified approximately equal to the 35% of the total energy loss. The remaining part (65%) is associated to the interlocking. Here the occurrence of lift-off for a limited time of the cycle of oscillation is responsible of the light jump in ₂₈₅ the FRFs (red curve of Figure 12).

The consideration here carried out suggest that proper design of the hook joint might increase the safety margins of the structure by bringing additional friction damping that other wise would be just localized at the interlocking.

5. CONCLUSIONS

₂₉₀ The analysis of the non-linear dynamic behavior of a stator vane segment in the presence of friction contacts is not a trivial task. This is mainly due to the huge number of physical DoFs required to approximate with high accuracy the motion at the contact interfaces. When such interfaces are not localized with respect to the physical domain of the components, as happens in the case of the ₂₉₅ hook joints, classical CMS reduction schemes preserving physical master DoFs are expensive from a computational point of view. For this reason, dedicated reduction techniques for contact interfaces have to be developed in order to efficiently handle the non-linear equations of motion. In this paper a novel

29

method to overcome the long computations of the frictionally damped non-linear systems with lap joints is presented. The method, which is based on the Gram-Schmidt Interface reduction technique[22], is here tailored to predict the non-linear forced response of a stator vane segment under the cyclic symmetry hypothesis. Results show the good accuracy of the method in spite of a dramatic reduction of the computational efforts.

References

[1] Pourkiaee S. M. and Zucca S., *A reduced order model for nonlinear dynamics of mistuned bladed disks with shroud friction contacts.* Journal of Engineering for Gas Turbines and Power 141.1 (2019): 011031.

[2] Bladh R., Castanier M. and Pierre C., 2003, *Effects of Multistage Coupling and Disk Flexibility on Mistuned Bladed Disk Dynamics* ASME Journal of Engineering for Gas Turbines and Power, 125(1), pp. 121130.

[3] Castanier, M. P., Ottarsson G. and Pierre C., *A reduced order modeling technique for mistuned bladed disks.* Journal of Vibration and Acoustics 119.3 (1997): 439-447.

[4] Battiato G., Firrone C. M. and Berruti T. M. 2017, *Forced Response of Rotating Bladed Disks: Blade Tip-Timing Measurements* Mechanical System and Signal Processing, 85, pp. 912926.

[5] Lassalle M. and Firrone C. M., *Nonlinear Forced Response of a Stator Vane with Multiple Friction Contact Using a Coupled Static/Dynamic Approach.* VII European Congress on Computational Methods in Applied Sciences and Engineering Crete Island, Greece, June, 2016.

[6] Firrone C. M. and Zucca S., *Modelling friction contacts in structural dynamics and its application to turbine bladed disks.* Numerical Analysis-Theory and Application. IntechOpen, 2011.

[7] Zucca S., Firrone C. and Gola M. 2012, *Numerical Assessment of Friction Damping at Turbine Blade Root Joints by Simultaneous Calculation of the Static and Dynamic Contact Loads* Nonlinear Dynamics, 67(3), pp. 19431955.

[8] Krack M., Panning L., Wallaschek J., Siewert C. and Hartung A., 2013, *Reduced Order Modeling Based on Complex Nonlinear Modal Analysis and Its Application to Bladed Disks With Shroud Contact* ASME Journal of Engineering for Gas Turbines and Power, 135.10, p. 102502.

32

[9] Sanliturk K. J., Ewins D. J., and Stanbridge A. B., *Underplatform dampers for turbine blades: theoretical modeling, analysis, and comparison with experimental data.* Journal of Engineering for Gas Turbine and Power 123.4 (2001): 919-929.

[10] Petrov E. P., and Ewins D. J., *Advanced modeling of underplatform friction dampers for analysis of bladed disk vibration.* Journal of Turbomachinery 129.1 (2007): 143-150.

[11] Firrone C. M., Berruti T. M., and Gola M. M., *On Force Control of an Engine Order-Type Excitation Applied to a Bladed Disk With Underplatform Dampers.* Journal of vibration and acoustic 135.4 (2013): 041103.

[12] Schwingshackl C. W., Petrov E. P., and Ewins D. J., *Effects of contact interface parameters on vibration of turbine bladed disks with underplatform dampers.* Journal of Engineering for Gas Turbines and Power. 134.3 (2012): 032507.

[13] Pennacchi P., Chatterton S., Bachschmid N., Pesatori E., and Turozzi G., *A model to study the reduction of turbine blade vibration using the snubbing mechanism.* Mechanical Systems and Signal Processing. 25 (2011), 12601275. doi:10.1016/j.ymssp.2010.10.006.

[14] Szwedowicz J., Visser R., SextroW., Masserey P. A. *On Nonlinear Forced Vibration of Shrouded Turbine Blades.* Journal of turbomachinery. 130.1 (2008)011002.

[15] Panning L., Popp K., Sextro W., Gotting F., Kayser A., and Wolter I., *Asymmetrical Underplatform Dampers in Gas Turbine Bladings: Theory and Application.* ASME Turbo Expo 2004: Power for Land, Sea, and Air. Americal Society of Mechanical Engineers, p. 269-280.

[16] Firrone C. M., Battiato G., and Epureanu B. I. *Modeling the Microslip in the Flange Joint and Its Effect on the Dynamics of a Multistage Bladed*

₃₆₅ *Disk Assembly.* Journal of Computational and Nonlinear Dynamics. 13.1 (2018): 011011.

[17] Battiato G., Firrone C. M., Berruti T. M., and Epureanu B. I. (2018). *Reduced Order Modeling for Multistage Bladed Disks With Friction Contacts at the Flange Joint.* Journal of Engineering for Gas Turbines and Power, ₃₇₀ 140(5), 052505.

[18] Castanier M. P., Yung-Chang T., and Pierre C., *Characteristic constraint modes for component mode synthesis.* AIAA journal 39.6 (2001): 1182-1187.

[19] Lindberg E., Horlin N. E., and Goransson P., (2013) *Component mode synthesis using undeformed interface coupling modes to connect soft and* ₃₇₅ *stiff substructures.* Shock and Vibration, 20(1), 157- 170.

[20] Holzwarth P., and Eberhard P., *Interface reduction for CMS methods and alternative model order reduction* IFAC-PapersOnLine, 2015, 48.1: 254-259.

[21] Kuether R. J., Allen M. S., and Hollkamp J. J., *Modal substructuring of geometrically nonlinear finite element models with interface reduction.* AIAA ₃₈₀ Journal, 2017, 1695-1706.

[22] Battiato, G., Firrone C. M., Berruti T. M., and Epureanu B. I., *Reduction and coupling of substructures via Gram Schmidt Interface modes.* Computer Methods in Applied Mechanics and Engineering, 336, 187-212.

[23] Battiato, G., Firrone C. M., *Reduced order modeling for forced response* ₃₈₅ *prediction of structures with large contact interfaces.* Proceedings of ISMA Conference, Leuven, Belgium (2018).

[24] Firrone C. M., and Battiato G., *A reliable pre-processing for the simulation of friction joints in turbomachineries and its validation: a case study with Policontact.* Proceedings of ASME Turbo Expo 2019: Turbomachin- ₃₉₀ ery Technical Conference and Exposition GT2019, Phoenix, Arizona, June, 2019.

[25] Tran, D. M., *Component Mode Synthesis Methods Using Interface Modes: Application to Structures with Cyclic Symmetry*, Computer & Structure, 79:209222, 2001.

[26] Craig R., and Bampton M., *Coupling of Substructures for Dynamic Analyses*, AIAA Journal 6.7 (1968): 1313-1319.

[27] Cameron T. M. and Griffin J. H., *An Alternating Frequency Time Domain Method for Calculating the Steady-State Response of Nonlinear Systems.* Journal of Applied Mechanics, 56(1), 149-154.

[28] Petrov E. P. and Ewins D. J., *Analytical Formulation of friction interface elements for analysis on nonlinear multi-harmonic vibrations of bladed discs.* ASME Turbo Expo 2002: Power for Land, Sea, and Air. American Society of Mechanical Engineers, 2002

[29] Gilbert Strang. *Introduction to linear algebra.* Wellesley, MA: Wellesley-Cambridge Press, 1993.

[30] Voormeeren, S. N. *Dynamic Substructuring Methodologies for Integrated Dynamic Analysis of Wind Turbines.* PhD thesis, Technische Universiteit Delft, 2012.